Proteome Science

RESEARCH

Open Access

NEK10 kinase ablation affects mitochondrial morphology, function and protein phosphorylation status

Andressa Peres de Oliveira[1,2], Claudia D. C. Navarro[3], Pedro Rafael F. Dias[1], Tania Arguello[2], Brittni R. Walker[2], Sandra R. Bacman[2], Lizandra Maia Sousa[4], Roger F. Castilho[3], Sílvio R. Consonni[4], Carlos T. Moraes[2*] and Jörg Kobarg[1*]

Abstract

Background NEK10, a serine/threonine/tyrosine kinase belonging to the NEK (NIMA-related kinases) family, has been associated with diverse cellular processes. However, no specific target pathways have been identified. Our previous work knocking down NEK10 in HeLa cells suggested a functional association with mitochondria, as we observed altered mitochondrial morphology, mitochondrial oxygen consumption, mtDNA integrity, and reactive oxygen species levels.

Methods To better understand this association, we studied human HAP1 cells fully knockout for NEK10 and confirmed that NEK10 has an important role in mitochondrial homeostasis.

We performed the study of mitochondrial respiration, mitochondrial morphology, mitochondrial mass, and mtDNA analysis. Additionally, we showed proteome and phosphoproteome data of crude mitochondrial fraction of Parental and NEK10 KO cells using liquid chromatography-mass spectrometry (LC–MS/MS).

Results In the absence of NEK10 several mitochondrial functions were disturbed. Moreover, proteome and phosphoproteome analyses of mitochondrial fractions showed that NEK10 alters the threonine phosphorylation status of several mitochondrial/endoplasmic reticulum components, including HSP60, NDUFB4, and TOM20. These changes impacted the steady-state levels of a larger group of proteins, preferentially involving respiratory complexes and autophagy pathways.

Conclusion We concluded that NEK10 plays a key role in mitochondrial function, possibly by modulating the phosphorylation status of mitochondrial proteins.

*Correspondence:
Carlos T. Moraes
cmoraes@med.miami.edu
Jörg Kobarg
jorgkoba@unicamp.br
Full list of author information is available at the end of the article

Introduction

By screening genetic factors that influence cell division in *Aspergillus nidulans*, Oakley and Moris identified the NIMA protein (encoded by *never-in-mitosis gene A*), which is the founding kinase of the NEK family (NIMA-related kinases). Human cells express eleven genes that encode NEK1 to NEK11 proteins [1, 2]. These NEK kinases were found to have important roles in mitosis and meiosis, primary ciliary, DNA damage response, centrosome organization, and splicing, among other functions. Additionally, NEKs are associated with several diseases [1, 2].

Mitochondrial homeostasis is modulated by several members of the NEK family, including NEK1 [3–5], NEK2 [6], NEK4 [7], NEK5 [8, 9], and NEK10 [10]. Besides energy production, mitochondria are involved in several cellular pathways, including Ca^{2+} homeostasis, cell death, aging, metabolic signaling, and chronic inflammation. Disruptions in mitochondrial homeostasis have been shown to contribute to metabolic disorders, neurodegeneration, and cancer [11].

Notably, the mammalian NEK10 is a serine/threonine/tyrosine kinase with a molecular weight of 133 kDa [1, 2], however, a shorter isoform (80 kDa) enriched in mitochondria has been reported [10]. NEK10 has a kinase domain in the center of the protein. It also contains a coiled-coil region, located near the kinase domain, and four armadillo motifs at the amino-terminal regulatory domain, which probably act in protein–protein interactions [1, 2]. Previous studies of NEK10 showed a role in ciliogenesis and ciliopathy and maintenance of the G2/M checkpoint following ultraviolet (UV) irradiation [12]. In addition, NEK10 kinase was reported to phosphorylate p53 [13] and the ryanodine receptor (RYR1) in the endoplasmic reticulum of muscle cells [14].

We have previously shown that the knockdown of NEK10 using siRNA in HeLa cells was associated with mitochondrial abnormalities [10]. In this study, we investigated a human haploid HAP1 cell line with a complete knockout of the *Nek10* gene. We confirmed defects in mitochondrial structure and function but also found that NEK10 phosphorylation regulates several mitochondrial proteins, which affects mitochondrial homeostasis and the levels of respiratory complexes and autophagy factors.

Material and Methods

Cell lines

The HAP1 cells are a near-haploid human cell line derived from the KBM-7 chronic myelogenous leukemia (CML) cell line (Horizon Cat #C631). The HAP1 Parental (Control) and NEK10 KO (Knockout) haploid cells were produced by CRISPR/Cas9 and obtained from New Horizon/Perkin (line HZGHC002995c011). The NEK10 gene was edited by CRISPR/Cas9 by New Horizon/Perkin Elmer. This specific region is a highly conserved nucleotide sequence among the NEK10 isoforms. The target transcript is NM_199347.

The Guide RNA Sequence are: TGCTTGATTGGA CGTTCAAA;

PCR Forward: CAGAGAAACAGCCAGATGAAG AAAG;

PCR Reverse: GTGCTTACTGAAACATCTGGTCAT T.

The NEK10 KO cells have a 35 bp (base pair) removal in the NEK10 KO gene compared with control cells (Parental) (see Supplemental Fig.S1).

For cell maintenance, Dulbecco's modified IMDM medium was used in the presence of 10% fetal bovine serum and antibiotics [1 ml fungizone (amphotericin, cat#15,290–018) and 300 µl Gibco gentamicin (cat#15,750–060) per 500 ml of media]. For HAP1 cells, in our experiments, we considered early cell passages less or equal to 25 cell passages and late cell passages more than 25 cell passages.

The human HeLa cell line was obtained from the ATCC and maintained as recommended. For cells maintenance, was used Dulbecco's modified DMEM medium in the presence of 10% fetal bovine serum and antibiotics [1 ml fungizone and 300 µl gentamicin per 500 ml of media].

For NEK10 knockdown we used a lentiviral system of short interfering RNAs (shRNAs): (shNEK89: 5'-CAT TGCCAGAACACATTATAT-3'; shNEK90: 5'GCCTCG TCCAGATATTGTAGAA-3'). The pLKO.1 empty vector was used as a control (pLKO.1) and the shRNAs were obtained from the RNAi Consortium (TRC, IRB-Barcelona, Spain). Lentiviruses carrying shRNAs were produced and collected at the Laboratory of Viral Vectors (LVV, LNBio / CNPEM-Campinas, SP, Brazil). Lentiviruses were transduced in HeLa cells in the presence of 1 µg/ml of polybrene and a complete medium for 24 h. For selection, was used puromycin (Sigma-Aldrich, St. Louis, MO, USA) at 3 µg/ml.

Oligonucleotides and Probes

For NEK10 knockout test—NEK10 F2 5'- TGTTATTCT CTCTCCTAGGG—3'; NEK10 F1 5'-CATTGTGTTATT CTCTCTCC -3'; NEK10 B2 5'- AGA-TATGTTAAATGG AGCCC-3'; NEK10 B1 5'- GAGCCCTTTGGAAACATA T—3'.

For Mycoplasma test – MycoFoward 5'-GTAATACAT AGGTCGCAAGCGTTATC-3'; MycoReverse5'-CAC CATCTGTCACTCTGTTAACCTC-3'.

For TaqMan-real time PCR of mtDNA quantification- ND1 Forward 5'-GAAGTCACCCTAGCCATC ATTC-3'; ND1 Reverse 5′-GCAGGAGTAATCAGAGGT

GTTC -3′; Probe ND15′-/5TET/AAGGGTGGA/ZEN/GAGGTTAAAGGAGCC/3IABkFQ/-3. COI Forward 5′-TTCTGACTCTTACCTCCCTCTC-3′; COI Reverse 5′-TGGGAGTAGTTCCCTGCTAA-3′; Probe COI 5′-/56FAM/TCCTACTCC/ZEN/TGCTCGCATCTGCTA/3IABkFQ/-3′. Actin Forward 5′-GTCACCGGAGTCCATCAC-3′; Actin Reverse 5′-GCCATGTACGTTGCTATCCA-3′, Probe Actin 5′-/5Cy5/TGCCAGTGGTACGGCCAGAG/3IAbRQSp/-3 [15].

Antibodies

Western blotting: Anti-NEK10 goat polyclonal (D-17; Santa Cruz Biotechnology cat#sc-103067); rabbit anti-ATAD3B (1:1000 Proteintech 16,610–1-A); mouse anti-total phosphothreonine (1:1000 Cell Signaling (42H4) 8954); mouse anti-total phospho serine Arg-X-Tyr/Phe-X-pSer (1:1000 Cell Signaling 2981); rabbit anti-total phospho Tyrosine (1:1000 Cell Signaling P-Tyr-1000 8954S); rabbit anti-HSP60 (1:1000 Cell signaling D6F1); mouse anti-TOM20 (1:1000) Santa Cruz SC17764; mouse anti-tubulin A (1:1000 Protein Tech 66,031–1); rabbit Anti-AIF (1:1000 Cell Signaling D39D2); mouse anti-complex III UQCRC2 (1:1000 Abcam ab14745); mouse anti-complex I NDUFA9 (1:1000 Abcam ab14713); mouse anti-SDHA (1:1000 Abcam ab 14,715); mouse anti-ATP5A (1:1000 Abcam abI5H4C4).

Immunoprecipitation: rabbit anti-TOM20 (1:2000 Cell Signaling D39D2); rabbit anti-HSP60 (1:2000 Cell signaling D6F1); rabbit anti-ATAD3B (1:2000 Proteintech 16,610–1-A).

Immunocytochemistry: rabbit anti-TOM20 (1:200 Cell Signaling D39D2); rabbit Anti-AIF (1:200 D39D2 Cell Signaling); Alexa Fluor anti-rabbit 488 (1:250 Invitrogen).

OXPHOS Reagents

Oligomycin, FCCP, antimycin A, and rotenone were supplied by the Seahorse OCR assay kit. Sodium pyruvate, glutamine, and glucose were obtained from Sigma/Aldrich.

Fluorescent Dyes

MitoBright Deep Red- MitoBright LT dyes MT10 (Dojindo Bio) are designed to be retained in the mitochondria for long-term visualization and it is not dependent on a strong membrane potential. TMRM—The MitoProbe TMRM Assay Kit M20036 contains tetramethylrhodamine methyl ester for detecting the mitochondrial membrane potential state (Thermofisher Scientific Inc.). MitoSox—MitoSOX Red super-oxide indicator M36008 (Thermofisher Scientific Inc.)

Zeocin Treatment

Cells were treated with 300 µg/ml zeocin for 3 h in culture medium, followed by 3 h recovery.

Genotyping the HAP1 NEK10 knockout cells by PCR

For each reaction, was added 5 µl of 10 × reaction buffer (Green Reaction Buffer Thermo Scientific); 20 ng of plasmid DNA; 1 µl of each oligonucleotide (10 µM); 1 µl dNTP (10 mM); 0.5 µl of Dream Taq polymerase (Thermo Scientific) and volume adjusted to 50 µl with MilliQ water. For the PCR reaction, the following parameters were used: 1 cycle of 95°C for 1 min, 33 cycles of 95°C for 30 s; 55 °C for 30 s; and 72°C for 1 min/ plasmid kb, and finally, 1 cycle of 72°C for 15 min. PCR products were analyzed is a 12% polyacrylamide DNA gel, electrophoresed in TBE buffer (Tris/Borate/EDTA, pH 8.0).

Mitochondrial respiration analysis

For HAP1 cells (Parental and NEK10 KO), we used the Seahorse XFp Analyzer (Agilent, CA), which measures extracellular O2 through fluorescence sensors. Cells were plated in XFp Seahorse-specific plates. The phenol-free Seahorse XF medium was supplemented with 10 mM glucose, 2 mM glutamine, and 1 mM sodium pyruvate. Inhibitors were used at the following concentration: 1 µM oligomycin; 1.5 µM FCCP; 0.5 µM antimycin/rotenone. The results were analyzed on Seahorse Wave Desktop Software 2.6.1.

For HeLa cells (pLKO, sh89, and sh90), was used the Seahorse XF24 Analyzer (Agilent, CA). Cells were plated in XF24 Seahorse-specific plates. DMEM medium without phenol was supplemented with 25 mM glucose and 4 mM glutamine. Inhibitors were used at the following concentration: 1 µM oligomycin; 500 nM FCCP; and 1 µM antimycin/rotenone for mitochondrial respiratory analyses. The results were analyzed on Seahorse Wave Desktop Software 2.6.1. Quantification of OCR values subtracted non-mitochondrial oxygen consumption values.

Transmission *Electron* Microscopy (TEM)

The HAP1 cells (Parental and NEK10 KO) or HeLa cells (pLKO, sh89, and sh90) cells were plated in 6-well plates. On the next day, cells were fixed with 2.5% glutaraldehyde in 0.1 M sodium cacodylate and 3 mM CaCl2 buffer for 5 min at room temperature, followed by a 1 h incubation on ice. After fixation, the samples were washed three times in 0.1 M sodium cacodylate and 3 mM CaCl2 buffer and post-fixed with 1% osmium tetroxide with 0.8% potassium ferrocyanide in 0.1 M sodium cacodylate

buffer (pH 7.4), for 30 min, and then block stained with 2% uranyl acetate on ice-cold overnight.

The cells were dehydrated with ethanol at 4ºC and infiltrated in Epon resin. After four changes of resin solution, a fifth change of resin was performed and immediately placed in a vacuum oven at 60 ∘C to be polymerized for 72 h.

Ultrathin sections were cut with a Leica Ultracut microtome, stained with 2% uranyl acetate and Reynolds lead citrate, and examined in a Tecnai G2 Spirit BioTWIN (FEI Company, Hillsboro, OR, USA). Supplemental figures were obtained with a LEO 906-Zeiss transmission electron microscope at an accelerating voltage of 60 kV. TEM was performed at the Electron Microscopy Laboratory of the Institute of Biology at the University of Campinas. Mitochondrial morphology analysis was performed using Image J2 software. Cristae number was quantified as the number cristae segments spanning the matrix. The statistical analyses were performed with GraphPad Prism, and t-test or one-way ANOVA depending on the number of groups. Tukey's test was employed for post hoc analysis.

Immunocytochemistry

Parental and NEK10 KO cells were plated in 24-well plates with coverslips previously sterilized with UVC. When the cells reached 70% confluence, immunocytochemistry was performed. The cells were fixed with 4% paraformaldehyde for 20 min at room temperature. Cells were washed with PBS 2×rapidly. After that, the cells were permeabilized with 0.1% Triton X-100 and again, washed with PBS for 2×quickly. Cells were blocked with 2% BSA for 10 min at room temperature. The coverslips with cells were incubated with a primary antibody (anti-AIF or anti TOM20) diluted in 0.2% BSA for 45 min at room temperature in a humid chamber. The cells were washed twice with PBS for 5 min, each wash. The cells were incubated with a specific secondary antibody for immunofluorescence diluted in 0.2% BSA for 45 min at room temperature in a humid chamber. Cells were washed twice with PBS for 5 min each. Coverslips were overlaid on slides with EverBriteTM Mounting Media with DAPI (Biotium Cat#23,004). The AIF immunofluorescence intensity was obtained by the Image J2 Software.

Flow Cytometry

For flow cytometry analysis, Parental and NEK10 KO cells were plated in 6-well plates one day before. On the day of the procedure, cells were treated or untreated (assay negative control). For mitochondrial membrane potential analysis was used 20 nM MitoProbe TMRM. For mitochondrial mass analysis was used 0.1 µmol/l MitoBright Deep Red. For mitochondrial superoxide, analysis was used 5 µM MitoSox and 20 µM Antimycin A. Cells were washed 1×with PBS, trypsinized, and the cell pellets were washed 2×with PBS. Cells were resuspended in 400 µl PBS with 2% fetal bovine serum and analyzed on the BD FACSAria TM Ilu Special Order System. For each analysis, were collected 50.000 events. The data were analyzed with the software FCS Express 7 at the Flow Cytometry Core at the University of Miami, Miller School of Medicine.

Real-Time qPCR

To determine the total levels of mtDNA present in the samples, we performed qPCR using TaqMan reagents (PrimeTime Std qPCR Assay, Integrated DNA Technologies). Samples were analyzed on the BioRad CFX96/C1000 qPCR instrument. The comparative cycle threshold (Ct) method was used to determine relative values, and total mtDNA levels were determined by comparing mtDNA ND1 (TET) or COX1 (FAM) with genomic DNA actin (Cy5). For the real-time cycle, the following protocol was used: 95º. C for 3 min at 95°. C for 0.15 min and 60°. C for 1 min for 39 cycles [15].

Crude Mitochondrial Fractionation

Parental and NEK10 KO cells in different passages were plated in six 175 cm2 flasks four days before the crude mitochondrial fractionation assay. On the day of the procedure, the cells were washed twice with PBS (1×Phosphate Buffered Saline—pH 7.4) and trypsinized. The pellet was washed twice with 1×chilled PBS, and the cells were kept at 4 °C. The pellet was resuspended in T-K-Mg solution [10 mM Tris–HCl pH 7.0; 10 mM KCl; 0.15 mM ice-cold MgCl2] containing protease inhibitors (cOmplete™ Protease Inhibitor Cocktail Sigma/Roche®) and phosphatase inhibitors (PhosStop Sigma/Roche®) and left on ice for 5 min. Cells were homogenized with 60 strokes in a mechanical homogenizer for cell lysis. Sucrose and Tris–HCl pH 7.0 were added to the homogenate for a final concentration of 0.25 M and 10 mM, respectively. Cells were centrifuged at 1500 g for 3 min at 4 °C to obtain the nucleic fraction. The supernatant was centrifuged at 8000 g for 10 min at 4ºC to obtain the cytoplasmic fraction (supernatant) and the mitochondrial fraction (pellet). Depending on the procedure, the mitochondrial fraction was resuspended in solution A [20 mM Tris HCl p7.2; 0.25 M sucrose; 40 mM KCl; 2 mM EDTA] to be kept at -80º C or lysed with RIPA buffer [30 mM HEPES, pH 7.4,150 mM NaCl, 1% Nonidet P-40, 0.5% sodium deoxycholate, 0.1% sodium dodecyl sulfate, 5 mM EDTA, (cOmplete™ Protease Inhibitor Cocktail Sigma/Roche®) and phosphatase inhibitors (PhosStop Sigma/Roche®)] for LC–MS/MS

experiments, or lysed with Cell Signaling Lysis Buffer for immunoprecipitation assays.

DNA Extraction

Parental and NEK10 KO cells were grown in T-25 flasks for two days, washed 2×with PBS, trypsinized, and centrifuged at 1000×g for 10 min, and the pellet was used for DNA extraction. The NucleoSpin Tissue XS kit from Macharey-Nagel Ref # 740,901.250 was used. The DNA extraction protocol was followed according to the manufacturer's specifications.

Mycoplasma test

Parental and NEK10 KO cells were grown in T-25 flasks for 5 days with antibiotic-free IMDM medium, washed 2×with PBS, trypsinized, and centrifuged at 1000×g for 10 min and the pellet was used for DNA extraction. After DNA extraction, the PCR reaction described below. For each reaction was added 1 µl of 10×reaction buffer (Green Reaction Buffer Thermo Scientific); 0.5 µl of each oligonucleotide (Myco F and R 10 µM); 1.6 µl of dNTP (10 mM); 0.1 µl of Dream Taq polymerase (Thermo Scientific) and the volume adjusted to 10 µl with MilliQ water. The following parameters were used: 1 cycle of 95ºC for 5 min, 32 cycles of 95ºC for 30 s; 65 °C for 1 min; and 72 °C for 1 min/ plasmid kb, and finally, 1 cycle of 72 °C for 5 min.

Analysis of Liquid Chromatography—Mass Spectrometry (LC-M/MS)

The protocol below was used at the Proteomics Core of the University of Florida in Jupiter, FL, USA. The statistical analysis and graphs were performed at the University of Miami.

Quantitative analysis of the TMT pro-6plex experiment was performed simultaneously with protein identification using Proteome Discoverer 2.5 (PD) software. The precursor and fragment ion mass tolerances were set to 10 ppm, and 0.6 Da, respectively); the enzyme was Trypsin with a maximum of 2 missed cleavages and FASTA files for Uniprot Human (UP000005640, downloaded on 9/14/2020) proteome, and common contaminants were used in SEQUEST searches. The impurity correction factors obtained from Thermo Fisher Scientific for the TMT 6plex kit were included in the search and quantification. The following settings were used to search the non-enriched sample data; dynamic modifications; Oxidation /+15.995 Da (M), Deamidated /+0.984 Da (N, Q), N-Terminal modification of Acetyl /+42.011 Da (N-Terminus), Met-loss / -131.040 Da (M), Met-loss+Acetyl / -89.030 Da (M) and static modifications of TMTpro /+304.207 Da (Any N-Terminus, K) and MMTS+45.988 Da (C). Only unique+Razor peptides were considered for quantification purposes. The percolator feature of PD was used to set a false discovery rate (FDR) of 0.01. The samples were normalized using the "Total Peptide Amount" option at PD2.5. The protein Abundance Based method was used to calculate the protein level ratios. Co-isolation threshold and SPS Mass Matches threshold were set to 50 and 65, respectively.

The following settings were used to search the phospho-enriched data; dynamic modifications; Oxidation /+15.995 Da (M), Deamidated /+0.984 Da (N, Q), Phospho /+79.966 Da (S, T, Y), N-Terminal modification of Acetyl /+42.011 Da (N-Terminus), Met-loss / -131.040 Da (M), Met-loss+Acetyl / -89.030 Da (M) and static modifications of TMT6plex /+229.163 Da (N-Terminus, K), MMTS /+45.988 Da (C). Only unique+Razor peptides were considered for quantification purposes. The percolator feature of Proteome Discoverer 2.5 was used to set a false discovery rate (FDR) of 0.01. IMP-ptmRS node (Taus et al. 2011) was used to calculate probability values for each putative phosphorylation site. The "Total Peptide Amount" normalization method was used to adjust for loading bias, and non-phosphorylated peptides were excluded from normalization and ratio calculation. The protein Abundance Based method was used to calculate the protein level ratios. Co-isolation and SPS Mass Matches thresholds were set to 50 and 0, respectively.

At the peptide level, peptide isoforms were defined by the Peptide Isoform Grouper node that summarized PSMs that share the same sequence and modifications. Phosphopeptide isoforms (PI) were further evaluated by removing not quantified or not phosphorylated PIs. At the peptide and protein levels, phospho-enriched and non-enriched samples were analyzed using the following statistical method. Contaminant proteins/peptides were excluded from the data set, and signal/noise values were normalized using log2 transformation. Statistical analysis was performed using paired T-Test with GraphPad Prism version 9.5 (Graph Pad Software, San Diego, CA, USA). Proteins changes with p-value < 0.05 were considered significant.

Immunoprecipitation

To perform immunoprecipitation, the mitochondrial pellet was lysed with cell lysis buffer (Cell Signaling®) containing protease inhibitors (cOmplete™ Protease Inhibitor Cocktail Sigma/Roche®) and phosphatase inhibitors (PhosStop Sigma/Roche®). The mitochondrial pellet was incubated with a specific primary antibody at a dilution of 1:2000. After 1 h on the shaking platform at 4 °C, G-Sepharose was added, followed by 1 h on the shaking platform at 4 °C. The G-Sepharose-Ac-protein complexes were obtained by centrifugation, washed with

lysis buffer for 5x, and the proteins extracted with Laemmli buffer and analyzed by Western Blotting.

Western Blotting

Protein concentrations were measured with Bio Rad's DC Protein Assay reagent. Proteins were added to 10% Mini-PROTEAN® TGX™ Precast Protein Gels, 10-well, 50 µl #456,103, and transferred to Trans-Blot Turbo Mini 0.2 µm PVDF Transfer Packs #1,704,156, the transfer was carried out in Trans-Blot Turbo Transfer System. Immunoblot analysis was performed with primary antibodies diluted in a blocking solution (2% bovine serum albumin and 0.02% sodium azide in PBS-buffered saline). Protein bands were detected with peroxidase-conjugated antibodies and visualized by ECL chemiluminescence (Amersham). The images were acquired with ChemiDoc MP Imaging System. The intensity of the bands were obtained by the Image J2 Software [16].

Pathway analyses

The pathway analyses (Reactome and GO [Gene Ontology] Biological Processes) of phosphoproteins and non-phosphoproteins were performed using the online tool Enrichr 27 [17] available at https://maayanlab.cloud/Enrichr. Enrichr analyses gene sets in several ontology databases.

Statistical analysis

Statistical analysis was performed using One-Way ANOVA, followed by Tukey's or Dunnett's Multiple Comparison Test, or the paired or unpaired T-Test. GraphPad Prism version 9.5 (Graph Pad Software, San Diego, CA, USA) was used for statistical analysis and graph design. The statistical analysis is shown in Mean with SD or with SEM and represented by * when it is considered significant, where p-value < 0.05 = *, *p*-value < 0.01 = **, *p*-value < 0.001 ***, and *p*-value < 0.0001 = ****.

Results

Genetic characterization of NEK10 Knockout cells

To confirm the Nek10 gene knockout in a HAP1 haploid human line, specific oligonucleotide primers (Forward: F1, F2, and Reverse: B1, B2) were designed to amplify approximately 150 bp of the NEK10 exon 4 that includes the 35 bp deleted region. We expected to amplify approximately 150 bp fragments from the Parental cell's DNA and fragments that were 35 bp shorter than the NEK10 KO cell's DNA. The amplification and analyses confirmed the expected gene deletion in the NEK10 KO cells (Supplemental Figures S1B-C).

Finally, we performed a western blot using a NEK10-specific antibody. As expected, NEK10 was only observed in the parental Hap1 line (Supplemental Figures S1D).

Mitochondrial respiration is decreased in NEK10 KO cells

To study the mitochondrial respiration of Parental and NEK10 KO cells we measured oxygen consumption rate (OCR) using a Seahorse XFp Analyzer (Fig. 1). The data were obtained after three independent experiments each one in triplicate. As we have only one NEK10 KO line, we used different cell passages as surrogates for biological replicates. Our results indicate that the NEK10 knockout in HAP1 cells strongly impairs mitochondrial respiration (Fig. 1A). Both basal and maximal OCR were decreased in the NEK10 KO cells (Figs. 1B-C). The fraction of OCR that was inhibited by oligomycin inhibition, which is an indirect estimation of ATP synthesis capacity (ATP-linked OCR), was also decreased in the NEK10 KO cells (Fig. 1E). OCR related to proton leak and spare respiratory capacity were not significantly different (Figs. 1D, F).

To complement this data, we also measured mitochondrial OCR in HeLa NEK10-knockdown cells (with the previously described stable shRNAs:sh89 and sh90) [10], and respective control.

The data presented in Supplemental Figure S2 were obtained for four biological replicates ($n = 4$) in quadruplicate. We used each replicate from a different cell passage. Supplemental Figures S2A-C show that the NEK10 depletion in HeLa cells compromised mitochondrial respiration. Basal and maximal OCR were lower for both NEK10 shRNA lines, but reached significance only for sh90 cells (Suppl. Fig S2D), which has a stronger knockdown [10]. OCR related to proton leak (Supp Fig S2E), ATP-linked OCR (Suppl. Fig S2F), and respiratory spare capacity (Suppl. Fig S2G) were also decreased in the sh90 NEK10 knockdown line. The magnitude of the changes in the two systems was similar, and intrinsic differences between HeLa and HAP1 could explain small variations.

HAP1 NEK10 KO cells have morphologically abnormal mitochondria

The decreased mitochondrial respiration of NEK10 knockout cells led us to investigate their mitochondrial morphology. Transmission electron microscopy (TEM) revealed changes in mitochondrial morphology in the HAP1 NEK10 KO cells (Fig. 2). The criteria used to classify the morphology were the mitochondrial shapes: spherical/fragmented (< 0.6 µm), or elongated/regular (≥ 0.6 µm) [10, 18]. Representative images for each cell (Parental and NEK10 KO) are shown in Fig. 2A and B.

We observed an increase in the number of spherical/fragmented mitochondria (red arrows) in NEK10 KO cells compared to the control cells, which showed more elongated mitochondria (green arrows) (Fig. 2A, B, G, and H). Figures 2C-D summarize the morphological analysis. The data indicate a prevalence of elongated mitochondria in Parental cells, as 86% are elongated/

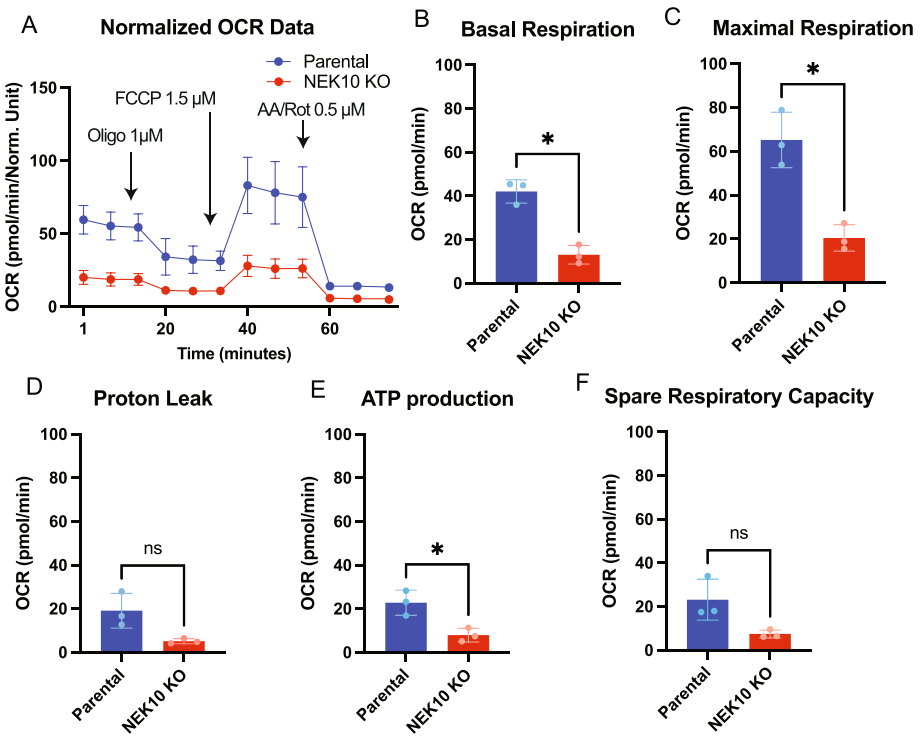

Fig. 1 Mitochondrial respiration of Parental and NEK10 KO cells. In **A**) The graph shows the OCR (Oxygen Consumption Rate) of Parental cells (in the blue line) and NEK10 KO cells (in the red line) by times in minutes. The black arrows show the time when the inhibitors were added with their respective concentration. **B** The graph shows the basal respiration of Parental and NEK10 KO cells. In **C**) Maximal OCR. **D** OCR related to proton leak. **E** ATP-linked OCR. **F** Spare Respiratory Capacity. Values were normalized by total proteins in µg/µl. The graphs show the results of 3 independent experiments ($n = 3$) in triplicate (3 different cell passages). The data was obtained with Seahorse XFp Analyzer – Agilent equipment and analyzed at Seahorse Wave desktop software. The statistical analyses were performed with GraphPad Prism and used the paired T-test * = $p < 0.05$. The graphs are shown in mean ± SD

regular and only 14% are spherical/fragmented mitochondria. On the other hand, the NEK10 KO cells show 60% elongated and 40% spherical mitochondria (Fig. 2C and D). The mitochondrial length (Fig. 2E), mitochondrial width (Fig. 2F), the surface of the mitochondrial area (Fig. 2G), and the number of mitochondrial cristae per mitochondrion (Fig. 2H) were also analyzed. We observed bigger mitochondria in Parental cells with an area, length, width, and cristae numbers higher than the mitochondria of NEK10 KO cells. Also, we found an increase in mitochondria number per cell area (Figs. 2A-C: 291 in KO vs. 161 in WT).

In addition to HAP1 cells, we also performed a similar analysis with the shRNA-depleted HeLa lines. Supplemental Figures S3A-C, illustrate images taken in TEM. In agreement with the NEK10 KO results, we observed elongated mitochondria in control cells with an area, length, width, and cristae number higher than the mitochondria of NEK10-knockdown cells. NEK10-knockdown cells have a larger number of spherical mitochondria compared to the control cells.

Supplemental Figure S3D-G shows that mitochondrial length (Suppl. Fig S3D), mitochondrial width (Suppl. Fig S3E), the surface of the mitochondrial area (Suppl. Fig S3F), and the number of mitochondrial cristae per mitochondrion (Suppl. Fig S3G) were consistently reduced in the NEK10 knockdown cells. The table in Suppl. Fig S3H summarizes the data. The results are similar to those observed for the HAP1 NEK10 KO cells, indicating a prevalence of elongated mitochondria in control cells, 87% are elongated in control cells (pLKO) whereas only 46–54% are elongated in the NEK10 depleted cells (Supp Fig S3H). The combined data of HeLa NEK10 knockdown and HAP1 KO cells strongly indicate that NEK10 kinase influences mitochondrial morphology in at least these two different cell types.

We also analyzed mitochondrial morphology by confocal microscopy using two different markers. Comparing Parental cells (Fig. 3A) with NEK10 KO cells (Fig. 3B), we found an increased Apoptosis-inducing factor (AIF) intensity signal in NEK10 KO cells, which agrees with the higher mass found in the NEK10 KO

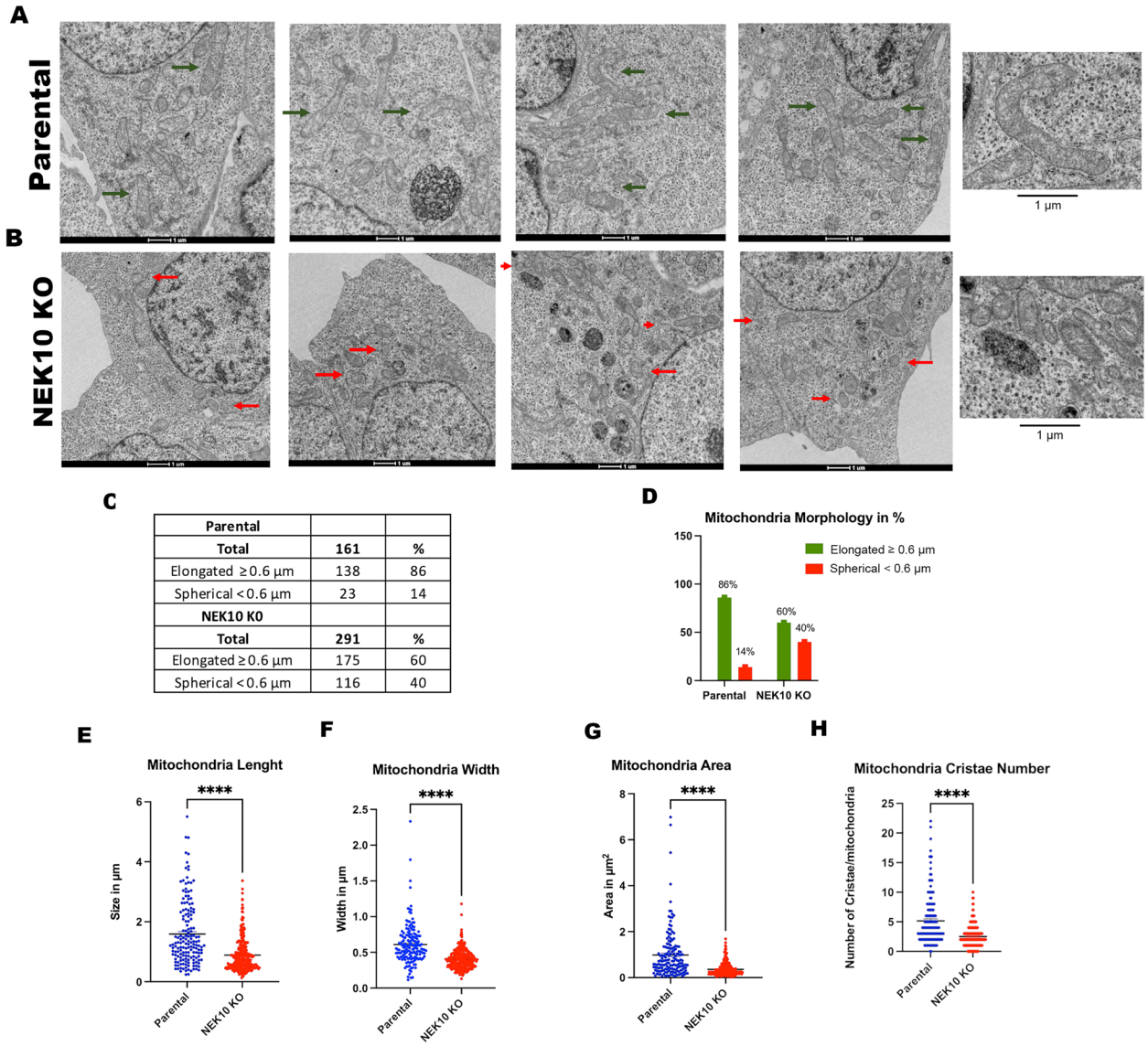

Parental		
Total	**161**	**%**
Elongated ≥0.6 µm	138	86
Spherical <0.6 µm	23	14
NEK10 K0		
Total	**291**	**%**
Elongated ≥0.6 µm	175	60
Spherical <0.6 µm	116	40

Fig. 2 Morphological analysis of mitochondria in HAP1 Parental and NEK10 KO cells by Transmission Electron Microscopy (TEM). Panel **A** shows four representative micrographs of the mitochondria of the Parental cells; and panel **B** shows four representative pictures of the mitochondria of NEK10 KO cells. The green arrows mark examples of normal/elongated mitochondria, whereas the red arrows mark examples of fragmented/spherical mitochondria. In total, 14 micrographs were analyzed for Parental cells and 15 images for NEK10 KO cells. A total of 161 mitochondria from Parental cells and 291 mitochondria from NEK10 KO cells were analyzed. **C** graph showing the mitochondrial length (size in µm); **D**) mitochondrial width (width in µm); **E**) mitochondrial area (area in µm2); **F**) number of mitochondrial cristae per mitochondrion. The mitochondrion was classified based on their mitochondrial morphology: spherical (< 6 µm), or elongated (> = 6 µm) (panels G and H). p-value < 0.05 = *, *p*-value < 0.01 = **, *p*-value < 0.001 ***, and *p*-value < 0.0001 = ****. The graphs are shown in Mean ± SEM

cells. The higher intensity signal in NEK10 KO cells was confirmed by quantification in ImageJ2 [16] (Fig. 3E). In addition to AIF, the expression of the TOM20 protein was also analyzed. As shown in Figs. 3C-D) there was a difference in the mitochondrial morphology between both cells. The NEK10 KO cells (Fig. 3D) show more distinct bright punctate signals (white arrows). Although there was a small apparent increase in the fluorescent signal of TOM20, proteome and western blot analysis (described below) showed that TOM20 was actually reduced in the Nek10 KO. We believe that this discrepancy is due to the fact that the TOM20 ICC signal is more condensed in the Nek10 KO, producing brighter spots. On the other hand, the signal is more diffuse in the control.

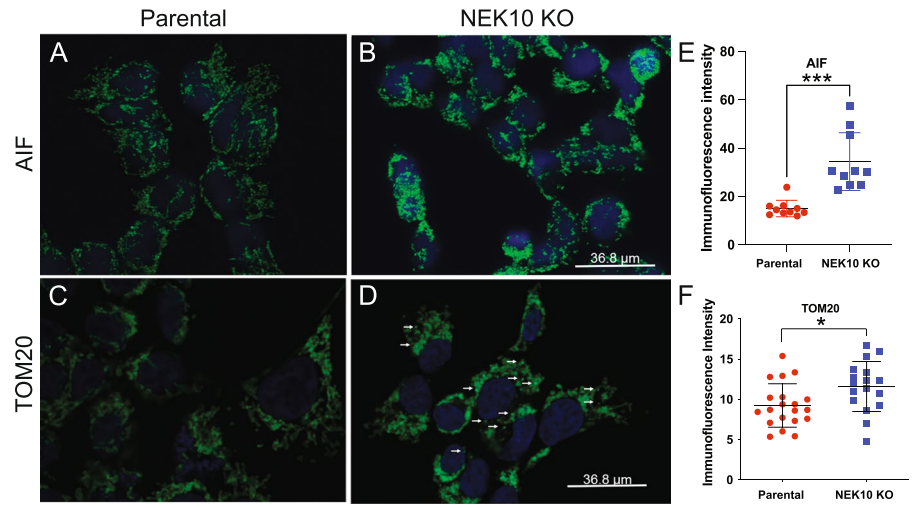

Fig. 3 Analysis of AIF and TOM20 protein expression of Parental and NEK10 KO cells by confocal microscopy. In panels, **A** and **C** show the Parental cells. Panels, **B** and **D** show the NEK10 KO cells. Panels **A-B** show AIF in green and the nuclear dye DAPI in blue. Panels **C-D** show TOM20 in green and the nuclear dye DAPI in blue In **E** and **F**, the graphs show the immunofluorescence intensity signal obtained by the Image J2 software [16]. Statistical analyses were performed with GraphPad Prism employing the unpaired t-test, where *p*-value < 0.05 = *, and *p*-value < 0.001 ***. The graphs show Mean ± SD. The images were obtained with the same intensity and brightness settings using a Leica Stellaris 5 confocal microscope

Higher signals of membrane potential-dependent dyes suggest increased mitochondrial mass in HAP-1 cells lacking NEK10

Mitochondrial mass was accessed by flow cytometry using MitoBright Deep Red, which is not dependent on membrane potential for retention [19, 20]. Figure 4A shows that NEK10 KO cells (red line) have a higher median fluorescence intensity than Parental Cells (blue line), suggesting an increase in mitochondrial mass in NEK10 KO cells.

A second analysis, using a mitochondrial membrane potential-dependent dye (TMRE) was also performed by FACS. Figure 4B shows that NEK10 KO cells have a higher median fluorescence intensity than Parental cells, which could be explained by the increased mitochondrial mass. This class of dye was used in "non-quenching mode" [21], as fluorescence intensity is reduced after FCCP treatment, an uncoupler that dissipates the mitochondrial membrane potential [22] (Suppl. Figure S4). Mitochondrial superoxide was measured (with MitoSOX) at baseline and after treatment with antimycin A, which stimulates superoxide production [23]. Figure 4C shows that the NEK10 KO cells have a higher median fluorescence intensity than Parental cells both at baseline and after AA treatment (Fig. 4D), which could be the result of increased mitochondrial mass as respiration was found to be decreased. However, we cannot rule out that the increased uptake of these dyes is the result of other inner membrane abnormalities.

Mitochondrial DNA levels are reduced in NEK10 KO after a DNA-damaging treatment.

As described above, our data suggested increased mitochondrial mass in NEK10 KO, but this was not reflected by increased mtDNA (Fig. 4E-F). Next, we investigated the influence of NEK10 on the mtDNA integrity after genotoxic stress promoted by zeocin treatment. The mtDNA of Parental and NEK10 KO cells (zeocin treated or not) was quantified by qPCR.

Zeocin is an antibiotic of the bleomycin class that causes double breaks in DNA [24, 25]. For this experiment, early and late passages were used for both cells (Parental and NEK10 KO cells). We quantified the mitochondrial gene COX1 (Fig. 4E) and the mitochondrial gene ND1 (Fig. 4F). MtDNA levels were determined by qPCR comparing mtDNA ND1 (TET) or COX1 (FAM) to the nuclear gene actin (Cy5) (see methods). The data showed a decrease in mtDNA levels in NEK10 KO cells compared to Parental cells upon zeocin treatment. This is in agreement with our previous work with HeLa cells, in which we found that the NEK10 knockdown decreased mtDNA integrity and increased the mtDNA damage after treatment with zeocin [10].

Phosphoproteome and Proteome analyses support a direct effect of NEK10 in mitochondria

The phosphoproteome and the proteome of crude mitochondrial fractions of Parental and NEK10 KO cells were analyzed by liquid chromatography-mass spectrometry (LC–MS/MS). The objective was to verify if the NEK10

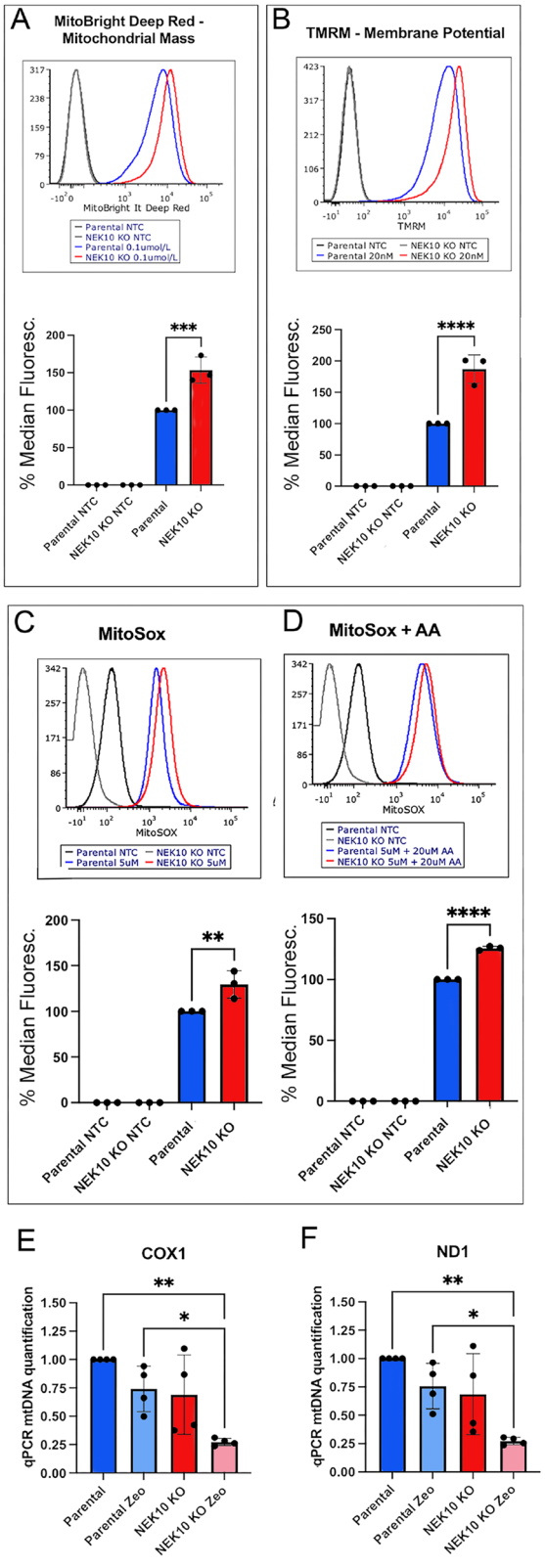

◀ **Fig. 4** Mitochondrial mass and superoxide analysis of Parental and NEK10 KO cells. **A** Histograms of flow cytometry analysis of cells treated or not with 0.1 µmol/l MitoBright Deep Red. **B** Histograms of flow cytometry analysis of cells treated or not with 20 nM MitoProbe TMRM. **C** Histograms of analysis of cells treated or not with MitoSox. In panel **D** cells were treated or not with 5 µM MitoSox + 20 µM Antimycin A (AA). The analysis was carried out on the BD FACSAria TM IIu Special Order System and the histograms were analyzed on FCS Express 7 software. **E** The graphs show the quantification of mtDNA levels of Parental and NEK10 KO cells treated with 300 µg/ml zeocin or untreated. Total mtDNA levels were determined by comparing mtDNA ND1 (TET) or COX1 (FAM) with genomic DNA, actin (Cy5). The graphs show the result of four different passages. Statistical analyses were performed with GraphPad Prism, employing one-way ANOVA tests followed by Tukey's test, where p-value < 0.05 = *, p-value < 0.01 = **, and p-value < 0.001 ***. The graphs are shown in Mean with SD

knockout would interfere with the phosphorylation and overall expression of mitochondria and the endoplasmic reticulum (ER) proteins. ER is closely associated with mitochondria at contact sites known as mitochondria-associated membranes (MAMs) [26].

The procedure to isolate crude mitochondrial preparations consisted of mechanical homogenization and differential centrifugation [27]. Crude mitochondrial fractions of early and late passages of Parental and NEK10 KO cells were prepared for LC–MS/MS. For Parental cells, we used passages p9, p10, and p40, and for NEK10 KO cells we used passages p7, p8, and p38. We consider passages p7, p8, p9, and p10 as early passages and p38 and p40 as late passages.

The relative purity of the sub-cellular fractions was analyzed by western blotting with anti-ATAD3B (a mitochondrial protein present mostly in the inner membrane) and anti-Tubulin A (a cytosolic marker, Supplemental Figure S5A-F). In addition, the knockout of NEK10 in these samples was confirmed by PCR (Supplemental Figure S5 G-H). We also made sure the cells were free of mycoplasma contamination (Supplemental Figure S5 I and J).

The mitochondrial fractions of each cell were analyzed by Liquid Chromatography-Mass Spectrometry (LC–MS/MS). The LC–MS/MS results were filtered for proteins related to mitochondria and the endoplasmic reticulum (Cellular Component filter available in the output table) to avoid analyzing contaminants from other cellular organelles, which could be present at variable levels. We analyzed the samples by comparing the corresponding passages of each cell line. For example, the variance of the NEK10 KO p7 was compared with Parental p9. Likewise, NEK10 KO p38 was compared to the Parental p40. These pairwise comparisons are appropriate because the respective samples spent similar times in

culture. In addition, the crude mitochondrial fractionation for these "similar passage samples" was performed at the same time.

Initially, we attempted to identify direct targets of NEK10 kinase responsible for the mitochondrial phenotypes observed by analyzing phosphoproteins that could be hypophosphorylated in the KO mitochondrial/ER samples. We found that among the altered phosphoproteins (p-value < 0.05, 65 proteins), 68% (44 phosphoproteins) had lower relative levels of phosphorylation in the NEK10 KO samples (Fig. 5A). These 44 proteins are shown in Fig. 5C and as heatmaps in Supplemental Figure S6. Although altered phosphorylation in factors such as TOM20 (translocase of the outer membrane), NDUFB4 (subunit of OXPHOS complex I), or HSP60 (mitochondrial quality control) could cause major mitochondrial phenotypic changes, additional proteins affecting Golgi/ER trafficking (ARHGAP21) or apoptosis (MCL1), could contribute as well.

Next, we analyzed the total proteome of the crude mitochondrial samples. Total proteins significant changes are shown in the volcano plot (Fig. 5B). We observed that 58% (100 proteins) had a higher abundance in Parental cells than in NEK10 KO cells. In total, there were 171 proteins with statistically significant differences ($p < 0.05$) between Parental and NEK10 KO. Figure 5D shows the relative abundance of a subset of these proteins ($p < 0.01$) to the parental samples. All significantly changed proteins ($p < 0.05$) are shown in Supplemental Fig.S7 Heatmaps are shown in Supplemental Figure S8.

We analyzed whether the significantly changed phosphoproteins and total proteins grouped into specific functional pathways. We used Enrichr, a web-based tool that allows access to several pathway databases [28]. The Reactome database showed autophagy, including mitophagy as a significantly altered pathway (Fig. 6A). Metabolism and response to stress were also significantly altered pathways. Go Biological Process database showed organelle organization, including Golgi/ER (Fig. 6A). Analysis of total altered proteome pathways showed that changes in components of oxidative phosphorylation, particularly complex I, were highly significant (Fig. 6B).

Analysis of the threonine, serine, and tyrosine phosphorylation of candidate mitochondrial proteins

The kinase NEK10 is a threonine, serine, and tyrosine kinase [13], for this reason, we investigated whether the total threonine, serine, or tyrosine phosphorylation of mitochondrial proteins was differentially modified. When the total crude mitochondria preparations were analyzed, there was a decrease in both phospho-Thr and in phosphor-Tyr from the NEK10KO samples. (Supplemental Figure S9).

Next, we immunoprecipitated specific candidate proteins, which were found to be affected by the LC–MS/MS analyses. These include HSP60 and TOM20. We also analyzed ATAD3 because our previous LC–MS/MS data on HeLa cells with NEK10 knockdown suggested that ATAD3 could be a NEK10 interactor [10]. Although we did not find significant changes in ATAD3 phosphorylation or levels in the present LC–MS/MS analysis, there was a clear trend for a decrease in protein levels in NEK10 KO samples (192/178/203 for NEK10 KO samples and 205/228/245 for Parental cells, $p = 0.06$; Supplemental Table 1).

Mitochondrial samples of early passages of Parental (p11) and NEK10 KO cells (p10), had these proteins immunoprecipitated. Western blots confirmed the immunoprecipitation of ATAD3, HSP60, and TOM20 (Fig. 7A-C). Next, immunoblotting of these immunoprecipitated with phosphor-specific antibodies was performed. Figures 7D and F show a decrease in threonine phosphorylation in ATAD3, HSP60, and TOM20 in NEK10 KO cells. The immunoprecipitated levels of HSP60 were slightly reduced (Fig. 7B), which could affect the decrease in phosphorylation observed by the western blot. However, a decrease in HSP60 phosphorylation was also observed by the phosphoproteome/proteome analyses.

As for serine (not shown) and tyrosine (Fig. 7E) phosphorylation, there were no significant differences between Parental and NEK10 KO cells in immunoprecipitated ATAD3, HSP60, or TOM20. Moreover, we did not detect changes in steady-state levels of any of these proteins in mitochondrial homogenates (Supplemental Fig.S10).

Discussion

NEK kinases and Mitochondrial function

Among the eleven human NEKs, the NEK1 [3–5], NEK2 [6], NEK4 [7], NEK5 [8, 9], and NEK10 [10] have been shown to influence mitochondrial homeostasis. The kinase NEK1 has been reported to phosphorylate the voltage-dependent anion channel 1 (VDAC1) [3, 4]. The knockout of NEK1 in HAP1 cells showed alterations in mitochondria homeostasis, such as a reduction in mitophagy. Also, the authors observed an increase in the total number of mitochondria, ROS levels, and mtDNA damage. In addition, NEK1 knockout impairs complex I activity [5]. NEK2 appears to regulate the splicing of pyruvate kinase M2 [6]. NEK4 depletion impairs mitochondrial respiration, decreases mtDNA integrity, and causes mitochondrial elongation [7]. In addition, cells overexpressing NEK4 increase mitochondrial respiration, mitochondrial membrane potential, and resistance to mitochondrial DNA damage. NEK5 kinase also has a

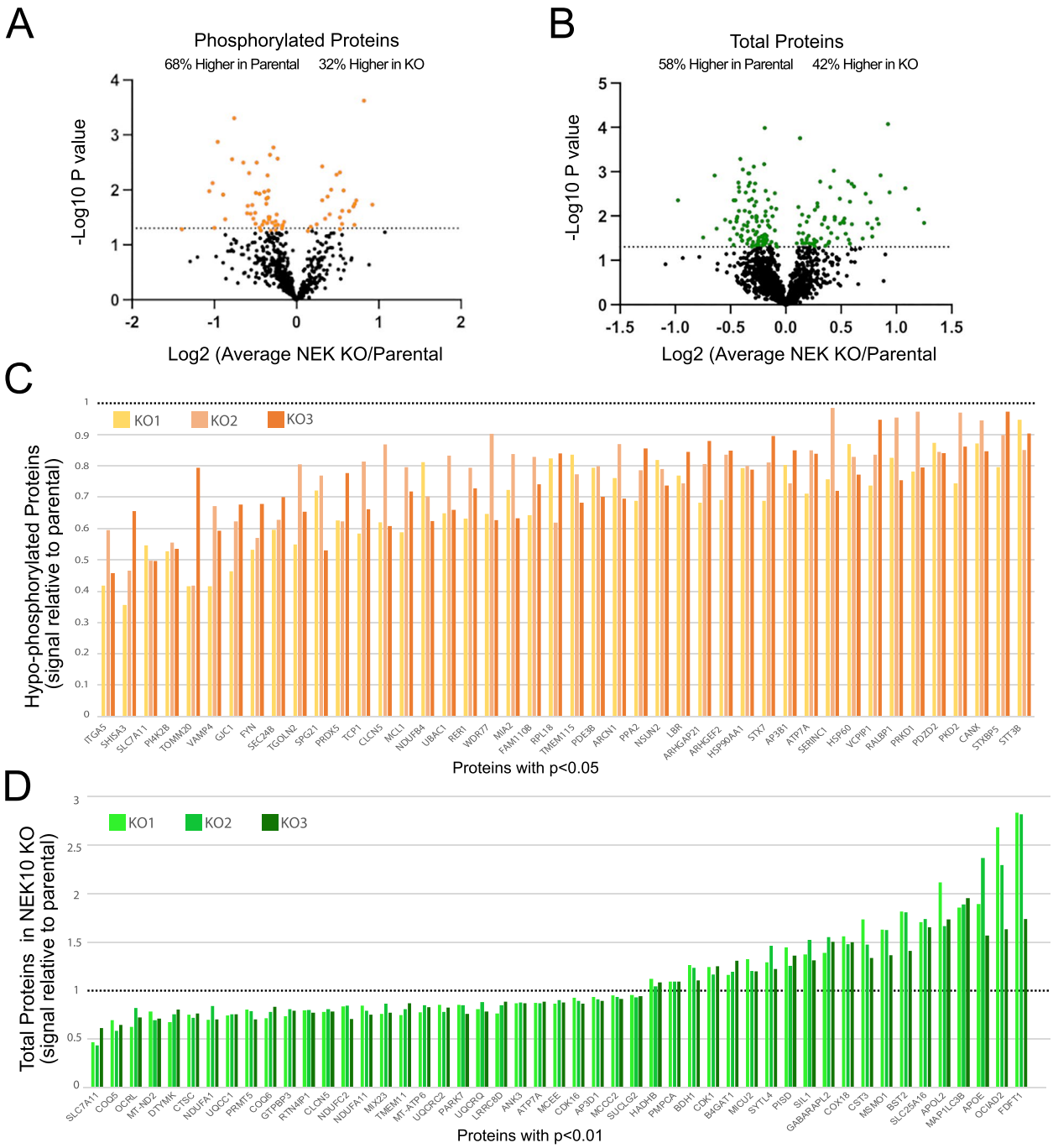

Fig. 5 Putative signal of phosphorylated mitochondrial and ER proteins altered in NEK10 KO cells. **A-B** Volcano plots show the p-value as log10 for Phospho- and Total proteome changes. **C** Proteins with significantly ($p < 0.05$) reduced phosphorylation in NEK10 KO (relative to control) crude mitochondria. **D** Subset of proteins with significantly altered levels ($p < 0.01$) in NEK10 KO (relative to control) crude mitochondria. Each NEK10 KO passage was normalized to its respective Parental control signal. All significantly changed ($p < 0.05$) proteins are shown in Supplemental Fig.S7

role in mitochondrial homeostasis. Cox11, MTX-2, and BCLAF1 were found to interact with NEK5 by yeast two-hybrid screens. NEK5 was reported to have a role in mitochondrial mass maintenance and mtDNA integrity after oxidative damage [8, 9].

Taken together, it is clear that a large branch of the NEK family has evolved to control key aspects of mitochondrial function, and NEK10 is part of this post-translational regulatory network.

Fig. 6 Pathway analyses of the phosphoproteome and proteome alterations in NEK10 KO crude mitochondria. We used Enrichr to investigate pathways significantly altered by the deletion of NEK10. **A** Phosphoproteome alterations (with $p < 0.05$) were analyzed in Reactome and GO (Gene Ontology) Biological Processes. **B** Total proteome alterations (with $p < 0.05$) were analyzed in Reactome and GO (Gene Ontology) Molecular Function. The bar graphs on the left shows the most significant pathways, with the altered genes indicated on the right. The normalized p value (q value) is shown on the left of both panels

Nek10 deletion produces overt mitochondrial abnormalities

Both in the Hap1 *Nek10* KO and in NEK10 knockdown in HeLa cells we found defective mitochondrial phenotypes, including decreased respiration, and increased mitochondrial fragmentation [10]. The magnitude of the changes in respiration in these two independent systems were very similar. The intrinsic differences between HeLa and HAP1 could explain their small variations. In the present work, we used a human HAP1 knockout cell line to completely eliminate NEK10, thereby avoiding any NEK10-related residual activity. Overexpression and even complementation of the KO with a transgene would be inappropriate controls, as the lack of endogenous regulation of kinases can have pleiotropic effects. The fact that two independent systems downregulating NEK10 gave similar phenotypes assures us that the observations made with the KO are due to the deletion of the *Nek10* gene.

Mitochondria morphology of HAP1 NEK10 KO as well as HeLa cells knockdown for NEK10 had marked increases in fragmented mitochondria. Although defects in a number of proteins related to mitochondrial fusion and fission could cause mitochondrial fragmentation, functional metabolic defects can also lead to morphological changes [29–31]. Along with the fragmentation we found evidence of increased mitochondrial mass in the NEK10 KO cells, which likely explains the increased membrane potential ($m\Delta\Psi$) and mitochondrial superoxide in NEK10 KO cells. It has been shown that FACS determinations of $m\Delta\Psi$ are influenced by the mitochondrial mass [32]. Likewise, the increased MitoSOX staining could be due to both increased mitochondrial mass and impaired OXPHOS. Although mtDNA copy number usually correlates with mitochondrial mass [29], it may not do so in abnormal conditions.

The most extreme case is observed in mtDNA depletion syndromes, where mitochondria proliferate, but mtDNA is markedly reduced or even absent [33]. The lack of correlation between mtDNA and mitochondria observed in NEK10 KO may be related to mtDNA replication factors [34] that directly or indirectly are affected by NEK10.

Phosphorylation defects in NEK10 KO cells

Our analyses of the phosphoproteome and the proteome of crude mitochondrial fractions of Parental and NEK10 KO cells suggested that the elimination of NEK10 affects the phosphorylation and expression of several mitochondria and endoplasmic reticulum (ER) proteins. Several proteins identified in the LC–MS/MS analyses showed differences in the putative signal of phosphorylated and total proteins. The phosphorylated putative signals of the mitochondrial 60 kDa heat shock protein and TOM20 showed reduced phosphorylation signal. Another example is the Complex I subunit NDUFB4, with a lower putative phosphorylated signal in NEK10 KO cells. Given the fact our data indicates the role of NEK10 in mitochondrial respiration, NEK10 could be contributing to complex I phosphorylation, and NDUFB4 would be a target candidate.

Our LC–MS/MS data indicate that the protein RER1 (Retention in Endoplasmic Reticulum Sorting Receptor 1) was hypophosphorylated in the NEK10 KO cells. The Golgi/ER pathway was a main pathway affected by the deletion of NEK10. Other affected pathways include: Autophagy/Mitophagy and Organelle Organization. Mitochondria function is greatly influenced by the ER and vice-versa, mostly through the mitochondrial-associated membrane (MAM) contact sites [35]. Interestingly, a recent publication showed that the NEK10 promotes the phosphorylation of the RYR1 receptor of the endoplasmic reticulum of muscle cells [14]. Therefore, the mitochondrial phenotypes observed in the Nek10 KO cells may be due to a combination of intra-mitochondrial and extra-mitochondrial phosphorylation alterations.

We also identified changes in the steady-state levels of several proteins related to the mitochondrial respiratory chain. The putative abundance signals of proteins related to Complex I, Complex III, and Complex V were decreased in NEK10 KO cells. Also, the levels of proteins related to the tricarboxylic acid cycle (TCA), such as Succinyl-CoA ligase, and PDK1 pyruvate dehydrogenase [36] were also decreased in the NEK10 KO. Accordingly, oxidative phosphorylation, and specifically complex I were significantly altered in the pathway analysis. All these data suggest a deficiency in mitochondrial OXPHOS in NEK10 KO cells.

(See figure on next page.)

Fig. 7 Analysis of total phosphorylation of threonine, serine, and tyrosine amino acids of candidate proteins. Immunoprecipitation of ATAD3, HSP60, and TOM20 from the crude mitochondrial fractionation of Parental and NEK10 KO cells (panels **A-C**). The lower part of the panels shows the total protein loading detected by the Bio-Rad Stain-Free Blot. The anti-rabbit antibody or anti-mouse IGG was used as the immunoprecipitation control. Anti-total threonine (**D**), and anti-total tyrosine (**E**) antibodies were used to detect phosphorylation by the western blotting of immunoprecipitates of ATAD3 (blue arrow), HSP60 (red arrow), and TOM20 (green arrow). Panel **F** shows the loading-normalized quantification of the blot from panel **D**. Panel **G** graphs the putative phosphorylation signals for these proteins from the LC–MS/MS analyses

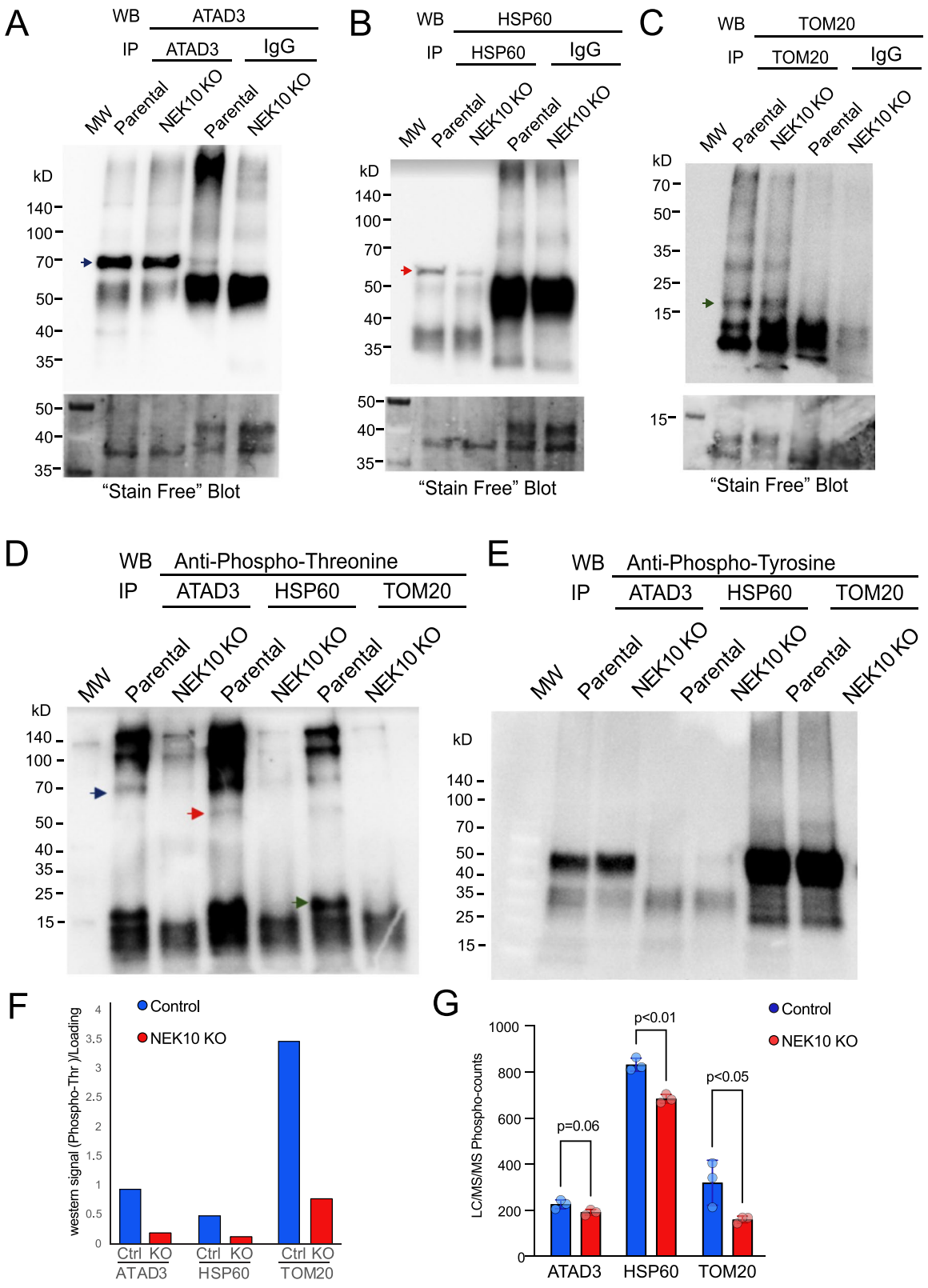

Fig. 7 (See legend on previous page.)

Although we did not focus on the "top hits", as any significantly altered protein could be relevant, we note that SLC7A11, an antiporter that mediates the uptake of extracellular cystine in exchange for glutamate, was one of the top hits in both in the hypophosphorylated and steady-state levels groups. Cystine is reduced to cysteine, which is a rate-limiting precursor in glutathione synthesis, which is an important antioxidant. Even though SLC7A11 is localized mostly at the plasma membrane, it is intrinsically linked to mitochondrial function [37]. It has been shown to play important functional roles by regulating the processes of redox homeostasis, metabolic flexibility, immune system function, and ferroptosis [38]. In sperm, SLC7A11 was shown to regulate both glutathione and glutamate metabolism [37].

Possibly related, another interesting protein found to be increased in NEK10 KO by LC–MS/MS is ornithine aminotransferase (OAT). OAT is a glutamate-metabolizing enzyme and we have previously found it to be a potential NEK10 interactor [10]. Therefore, glutamate metabolism, which is important for OXPHOS function and redox control could be one of the key pathways regulated by NEK10.

Concerning proteins directly involved in mitochondrial morphology, the mitochondrial fission factor (MFF) was among the significantly changed proteins (Supplemental Fig.S7). MFF is an essential factor in the mitochondrial recruitment of Drp1. Drp1 mediates mitochondrial fission [39]. Interestingly, the MFF overall signal was increased in NEK10 KO cells, suggesting that it could increase Drp1 recruitment.

The levels of proteins involved in mitochondrial DNA repair, such as Poly [ADP-ribose] polymerase 1 [40], DNA ligase 3 [41], and DNA mismatch repair protein Msh6 [42] were also increased in NEK10 KO cells. This suggests more mtDNA damage (or less effective repair) in the absence of NEK10 protein, which agrees with what we observed upon zeocin treatment.

Given the fact, that NEK10 is a threonine, serine, and tyrosine kinase [13], we investigated the total threonine, serine, and tyrosine phosphorylation of mitochondrial proteins ATAD3, HSP60, and TOM20. The analysis of the phosphoproteins data obtained by LC–MS/MS revealed that HSP60 and TOM20 proteins were hypophosphorylated in NEK10 KO cells. The mitochondrial chaperone Heat Shock Protein 60 (HSP60) has an essential role in protein folding and mitochondrial homeostasis. Mutations in the Hsp60 gene are related to neuropathies and paraplegias [43]. In addition, HSP60 participates in the cross-talk between mitochondria and endoplasmic reticulum during stress conditions [44]. HSP60 has many potential phosphorylation sites, which seem to affect its function [45]. TOM20 has a critical role in the import of mitochondrial proteins [46]. Its phosphorylation has been studied in yeast, where CK2 is the main kinase involved [47]. According to our previous LC–MS/MS data published in 2020 [10], the protein ATAD3 could be an NEK10 interactor. ATAD3 has a major role in regulating mitochondrial morphology [48].

Although our data showed a decrease in both phospho-Thr and phopho-Tyr when the NEK10 total KO crude prep was subjected to western blots using phosphor-AA specific antibodies, we could identify only a reduction in threonine phosphorylation in the three candidate mitochondrial proteins: ATAD3, HSP60, and TOM20. The western blot data was supported by the LC–MS/MS data for HSP60 and TOM20. Phosphorylation of ATAD3 was also reduced in the LC–MS/MS, but the difference was short of significance ($p=0.06$). Taken together, these results suggest that NEK10 acts in a pleiotropic manner controlling mitochondrial function, directly or indirectly. The morphological changes observed in the NEK10 KO cells could be explained by the effect in these proteins. HSP60 and TOM20 would affect a large number of mitochondrial proteins, including the ones associated with OXPHOS or mitochondrial dynamics. ATAD3 has a direct role in mitochondrial morphology.

Concluding remarks: Nek10 deletion and mitochondrial function

The data obtained from this work suggest the role of NEK10 in mitochondrial homeostasis. Targets of phosphorylation are likely multiple, and in different cellular compartments, including endosomes, ER, and mitochondria. Previous work has shown that NEK10 has alternative isoforms, some of which are enriched in mitochondria [10]. The present results showed that mitochondrial targets include HSP60, TOM20, NDUFB4, and likely ATAD3, but other mitochondrial- and ER-related proteins also seem to have their phosphorylation status altered by NEK10 ablation. Our data suggest that threonine and tyrosine phosphorylation are the prominent modifications associated with NEK10 in mitochondria.

Interestingly, missense mutations in NEK10 have been associated with bronchial ciliopathy in humans [49]. Although it is not clear why phenotypes in other tissues were not described in patients, mitochondrial function is critical for cilia movement [50]. The modulatory role of NEK10 in mitochondrial function may compound with other of its pleiotropic functions (e.g. regulating cilia size) in defining clinical phenotypes associated with hypomorphic missense mutations.

In conclusion, deletion of Nek10 had a major impact on the levels of numerous mitochondrial proteins, particularly those associated with respiratory complexes and autophagy pathways. Thus, it can be inferred that NEK10

plays a crucial role in maintaining mitochondrial function, potentially through the regulation of phosphorylation of mitochondrial proteins.

Abbreviations

OXPHOS	Oxidative Phosphorylation
NEK10	Nima-related kinase 10
OCR	Oxygen Consumption Rate
mΔΨ	Mitochondrial membrane potential

Supplementary Information

The online version contains supplementary material available at https://doi.org/10.1186/s12953-024-00234-z.

Supplementary Material 1.

Supplementary Material 2.

Acknowledgements
We thank Fapesp.

Authors' contributions
APO, JK and CTM wrote the main manuscript. APO prepared all figures. All authors reviewed, improved the manuscript.

Funding
This research was funded by FAPESP (Fundação de Amparo à Pesquisa do Estado de São Paulo) through "Projeto Temático" n. 2017/03489–1 and 2017/17728–8. Fellowships: FAPESP Brazilian National Fellowship n. 2020/07006–8 and 2019/20855–7 (to APO and CDCN); and Research International Fellowship—BEPE (Bolsa Estágio de Pesquisa no Exterior) FAPESP n. 2021/07071–7. The work in the Moraes laboratory was funded by National Institute of Health (NIH) Grants 5R01EY010804 and 1R01NS079965, the Florida Biomedical Foundation (21K05), the Muscular Dystrophy Association (MDA 964119) and the Army Research Office (W911NF-21–1-0248).

Availability of data and materials
No datasets were generated or analysed during the current study.

Declarations

Ethics approval and consent to participate
This work did not involve any human subjects or animal studies research.

Competing interests
The authors declare no competing interests.

Author details
[1]Faculdade de Ciências Farmacêuticas, Universidade Estadual de Campinas, Rua Cândido Portinari, 200 Cidade Universitária Zeferino Vaz, Campinas, SP CEP 13083-871, Brazil. [2]Department of Neurology, Miller School of Medicine, University of Miami, Miami, FL, USA. [3]Departamento de Patologia, Faculdade de Ciências Médicas, Universidade Estadual de Campinas, Campinas, SP, Brazil. [4]Departamento de Bioquímica E Biologia Tecidual, Instituto de Biologia, Universidade Estadual de Campinas, Campinas, SP, Brazil.

Received: 21 January 2024 Accepted: 1 October 2024
Published online: 08 October 2024

References

1. Peres de Oliveira A, Issayama LK, Pavan ICB, Silva FR, Melo-Hanchuk TD, Simabuco FM, et al. Checking NEKs: Overcoming a Bottleneck in Human Diseases. Molecules. 2020 [cited 2020 Apr 14];25:1778. Available from: https://www.mdpi.com/1420-3049/25/8/1778.
2. Pavan ICB, Peres de Oliveira A, Dias PRF, Basei FL, Issayama LK, Ferezin C de C, et al. On Broken Ne(c)ks and Broken DNA: The Role of Human NEKs in the DNA Damage Response. Cells 2021, Vol 10, Page 507. 2021 [cited 2021 Dec 3];10:507. Available from: https://www.mdpi.com/2073-4409/10/3/507/htm.
3. Chen Y, Craigen WJ, Riley DJ. Nek1 regulates cell death and mitochondrial membrane permeability through phosphorylation of VDAC1. Cell Cycle. 2009;8:257–67.
4. Chen Y, Gaczynska M, Osmulski P, Polci R, Riley DJ. Phosphorylation by Nek1 regulates opening and closing of voltage dependent anion channel 1. Biochem Biophys Res Commun. 2010;394:798–803.
5. Martins MB, Perez AM, Bohr VA, Wilson DM, Kobarg J. NEK1 deficiency affects mitochondrial functions and the transcriptome of key DNA repair pathways. Mutagenesis. 2021 [cited 2023 Feb 6];36:223–36. Available from: https://pubmed.ncbi.nlm.nih.gov/33740813/.
6. Gu Z, Xia J, Xu H, Frech I, Tricot G, Zhan F. NEK2 Promotes Aerobic Glycolysis in Multiple Myeloma Through Regulating Splicing of Pyruvate Kinase. J Hematol Oncol. 2017;1–11. Available from: https://doi.org/10.1186/s13045-017-0392-4.
7. Basei FL, de Castro Ferezin C, Rodrigues de Oliveira AL, Muñoz JP, Zorzano A, Kobarg J. Nek4 regulates mitochondrial respiration and morphology. FEBS J. 2022 [cited 2023 Feb 6];289:3262–79. Available from: https://pubmed.ncbi.nlm.nih.gov/34986513/.
8. Ferezin C de C, Basei FL, Melo-Hanchuk TD, de Oliveira AL, Peres de Oliveira A, Mori MP, et al. NEK5 interacts with LonP1 and its kinase activity is essential for the regulation of mitochondrial functions and mtDNA maintenance. FEBS Open Bio. 2021 [cited 2023 Feb 6];11:546–63. Available from: https://pubmed.ncbi.nlm.nih.gov/33547867/.
9. Melo Hanchuk TD, Papa PF, La Guardia PG, Vercesi AE, Kobarg J. Nek5 interacts with mitochondrial proteins and interferes negatively in mitochondrial mediated cell death and respiration. Cell Signal. 2015;27:1168–77.
10. Peres de Oliveira A, Basei FL, Slepicka PF, de Castro Ferezin C, Melo-Hanchuk TD, de Souza EE, et al. NEK10 interactome and depletion reveal new roles in mitochondria. Proteome Sci. 2020 [cited 2020 Apr 29];18:4. Available from: https://proteomesci.biomedcentral.com/articles/10.1186/s12953-020-00160-w.
11. SJ A, PR F. Mitochondria in Health and Disease. Cells. 2019 [cited 2021 Dec 3];8:1–620. Available from: https://pubmed.ncbi.nlm.nih.gov/31284394/.
12. Moniz LS, Stambolic V. Nek10 mediates G2/M cell cycle arrest and MEK autoactivation in response to UV irradiation. Mol Cell Biol. 2011;31:30–42. Available from: http://www.pubmedcentral.nih.gov/articlerender.fcgi?artid=3019845&tool=pmcentrez&rendertype=abstract.
13. Haider N, Dutt P, Van De Kooij B, Yaffe M. NEK10 tyrosine phosphorylates p53 and controls its transcriptional activity. 2019.
14. Yan W, Cao M, Ruan X, Jiang L, Lee S, Lemanek A, et al. Cancer-cell-secreted miR-122 suppresses O-GlcNAcylation to promote skeletal muscle proteolysis. Nat Cell Biol. 2022 [cited 2022 Jul 30];24:793–804. Available from: https://pubmed.ncbi.nlm.nih.gov/35469018/.
15. Bacman SR, Kauppila JHK, Pereira C V., Nissanka N, Miranda M, Pinto M, et al. MitoTALEN reduces mutant mtDNA load and restores tRNAAla levels in a mouse model of heteroplasmic mtDNA mutation. Nat Med. 2018 [cited 2022 Jul 25];24:1696. Available from: https://www.pmc/articles/PMC6942693/.
16. Schindelin J, Arganda-Carreras I, Frise E, et al. Fiji: an open-source platform for biological-image analysis. Nat Methods. 2012;9:676–82. https://doi.org/10.1038/nmeth.2019.
17. Kuleshov M V., Jones MR, Rouillard AD, Fernandez NF, Duan Q, Wang Z, et al. Enrichr: a comprehensive gene set enrichment analysis web server 2016 update. Nucleic Acids Res. 2016 [cited 2024 Jan 10];44:W90–7. Available from: https://pubmed.ncbi.nlm.nih.gov/27141961/.
18. Knott AB, Perkins G, Schwarzenbacher R, Bossy-Wetzel E. Mitochondrial fragmentation in neurodegeneration. Nat Rev Neurosci 2008 97. 2008 [cited 2023 Feb 20];9:505–18. Available from: https://www.nature.com/articles/nrn2417.
19. Sun L, Morikawa K, Sogo Y, Sugiura Y. MHY1485 enhances X-irradiation-induced apoptosis and senescence in tumor cells. J Radiat Res. 2021 [cited 2022 Aug 26];62:782–92. Available from: https://pubmed.ncbi.nlm.nih.gov/34265852/.
20. MitoBright LT Deep Red | Dojindo. [cited 2022 Aug 26]. Available from: https://www.dojindo.eu.com/MitoBright-LT-Deep-Red.aspx.

21. Ward MW, Rego AC, Frenguelli BG, Nicholls DG. Mitochondrial Membrane Potential and Glutamate Excitotoxicity in Cultured Cerebellar Granule Cells. J Neurosci. 2000 [cited 2024 Jul 21];20:7208. Available from: https://www.pmc/articles/PMC6772767/.
22. Benz R, McLaughlin S. The molecular mechanism of action of the proton ionophore FCCP (carbonylcyanide p-trifluoromethoxyphenylhydrazone). Biophys J. 1983 [cited 2024 Jul 28];41:381–98. Available from: https://pubmed.ncbi.nlm.nih.gov/6838976/.
23. Quinlan CL, Gerencser AA, Treberg JR, Brand MD. The Mechanism of Superoxide Production by the Antimycin-inhibited Mitochondrial Q-cycle. J Biol Chem. 2011 [cited 2024 Jan 11];286:31361. Available from: https://www.pmc/articles/PMC3173136/.
24. Hwang J, Kim YY, Huh S, Shim J, Park C, Kimm K, et al. The time-dependent serial gene response to zeocin treatment involves caspase-dependent apoptosis in HeLa cells. Microbiol Immunol. 2005;49:331–42.
25. Chankova SG, Dimova E, Dimitrova M, Bryant PE. Induction of DNA double-strand breaks by zeocin in Chlamydomonas reinhardtii and the role of increased DNA double-strand breaks rejoining in the formation of an adaptive response. Radiat Environ Biophys. 2007 [cited 2022 Aug 26];46:409–16. Available from: https://pubmed.ncbi.nlm.nih.gov/17639449/.
26. Carreras-Sureda A, Kroemer G, Cardenas JC, Hetz C. Balancing energy and protein homeostasis at ER-mitochondria contact sites. Sci Signal. 2022 [cited 2022 Aug 2];15:eabm7524. Available from: https://www.science.org/doi/10.1126/scisignal.abm7524.
27. Wieckowski MR, Wojtczak L. Isolation of crude mitochondrial fraction from cells. Methods Mol Biol. 2015 [cited 2022 Aug 23];1241. Available from: https://pubmed.ncbi.nlm.nih.gov/25308483/.
28. Xie Z, Bailey A, Kuleshov M V., Clarke DJB, Evangelista JE, Jenkins SL, et al. Gene Set Knowledge Discovery with Enrichr. Curr Protoc. 2021 [cited 2024 Jan 11];1:e90. Available from: https://onlinelibrary.wiley.com/doi/full/10.1002/cpz1.90.
29. Babbar M, Saeed Sheikh M. Metabolic Stress and Disorders Related to Alterations in Mitochondrial Fission or Fusion. Mol Cell Pharmacol. 2013 [cited 2023 Mar 30];5:109. Available from: https://www.pmc/articles/PMC3921894/.
30. Galloway CA, Yoon Y. Mitochondrial Morphology in Metabolic Diseases. Antioxid Redox Signal. 2013 [cited 2023 Mar 30];19:415. Available from: https://www.pmc/articles/PMC3700066/.
31. Samant SA, Zhang HJ, Hong Z, Pillai VB, Sundaresan NR, Wolfgeher D, et al. SIRT3 deacetylates and activates OPA1 to regulate mitochondrial dynamics during stress. Mol Cell Biol. 2014 [cited 2022 Feb 3];34:807–19. Available from: https://pubmed.ncbi.nlm.nih.gov/24344202/.
32. Yu W, Wang X, Zhao J, Liu R, Liu J, Wang Z, et al. Stat2-Drp1 mediated mitochondrial mass increase is necessary for pro-inflammatory differentiation of macrophages. Redox Biol. 2020 [cited 2024 Jan 11];37. Available from: https://pubmed.ncbi.nlm.nih.gov/33080440/.
33. El-Hattab AW, Scaglia F. Mitochondrial DNA depletion syndromes: review and updates of genetic basis, manifestations, and therapeutic options. Neurotherapeutics. 2013 [cited 2024 Jan 11];10:186–98. Available from: https://pubmed.ncbi.nlm.nih.gov/23385875/.
34. Gupta R, Kanai M, Durham TJ, Tsuo K, McCoy JG, Kotrys A V., et al. Nuclear genetic control of mtDNA copy number and heteroplasmy in humans. Nat 2023 6207975. 2023 [cited 2024 Jan 11];620:839–48. Available from: https://www.nature.com/articles/s41586-023-06426-5.
35. Tubbs E, Rieusset J. Metabolic signaling functions of ER-mitochondria contact sites: role in metabolic diseases. J Mol Endocrinol. 2017 [cited 2024 Jan 11];58:R87–106. Available from: https://pubmed.ncbi.nlm.nih.gov/27965371/.
36. Stacpoole PW. Therapeutic Targeting of the Pyruvate Dehydrogenase Complex/Pyruvate Dehydrogenase Kinase (PDC/PDK) Axis in Cancer. J Natl Cancer Inst. 2017 [cited 2023 Feb 9];109. Available from: https://pubmed.ncbi.nlm.nih.gov/29059435/.
37. Ortiz-Rodríguez JM, Martín-Cano FE, Gaitskell-Phillips G, Silva A, Tapia JA, Gil MC, et al. The SLC7A11: sperm mitochondrial function and non-canonical glutamate metabolism. Reproduction. 2020 [cited 2024 Jan 11];160:803–18. Available from: https://pubmed.ncbi.nlm.nih.gov/33112766/.
38. Jyotsana N, Ta KT, DelGiorno KE. The Role of Cystine/Glutamate Antiporter SLC7A11/xCT in the Pathophysiology of Cancer. Front Oncol. 2022 [cited 2024 Jan 11];12. Available from: https://pubmed.ncbi.nlm.nih.gov/35280777/.
39. Otera H, Wang C, Cleland MM, Setoguchi K, Yokota S, Youle RJ, et al. Mff is an essential factor for mitochondrial recruitment of Drp1 during mitochondrial fission in mammalian cells. J Cell Biol. 2010 [cited 2023 Feb 9];191:1141. Available from: https://www.pmc/articles/PMC3002033/.
40. Herrmann GK, Russell WK, Garg NJ, Yin YW. Poly(ADP-ribose) polymerase 1 regulates mitochondrial DNA repair in an NAD-dependent manner. J Biol Chem. 2021 [cited 2023 Feb 9];296. Available from: http://www.jbc.org/article/S0021925821000788/fulltext.
41. Simsek D, Jasin M. DNA ligase III: A spotty presence in eukaryotes, but an essential function where tested. Cell Cycle. 2011 [cited 2023 Feb 9];10:3636. Available from: https://www.pmc/articles/PMC3266004/.
42. Mason PA, Matheson EC, Hall AG, Lightowlers RN. Mismatch repair activity in mammalian mitochondria. Nucleic Acids Res. 2003;31(3):1052–8. https://doi.org/10.1093/nar/gkg167.
43. Rodriguez A, Von Salzen D, Holguin BA, Bernal RA. Complex Destabilization in the Mitochondrial Chaperonin Hsp60 Leads to Disease. Front Mol Biosci. 2020 [cited 2024 Jan 11];7. Available from: https://pubmed.ncbi.nlm.nih.gov/32766281/.
44. Xiao T, Liang X, Liu H, Zhang F, Meng W, Hu F. Mitochondrial stress protein HSP60 regulates ER stress-induced hepatic lipogenesis. J Mol Endocrinol. 2020 [cited 2024 Jan 11];64:67. Available from: https://www.pmc/articles/PMC6993205/.
45. Caruso Bavisotto C, Alberti G, Vitale AM, Paladino L, Campanella C, Rappa F, et al. Hsp60 Post-translational Modifications: Functional and Pathological Consequences. Front Mol Biosci. 2020 [cited 2024 Jan 11];7. Available from: https://pubmed.ncbi.nlm.nih.gov/32582761/.
46. Bhagawati M, Arroum T, Webeling N, Montoro AG, Mootz HD, Busch KB. The receptor subunit Tom20 is dynamically associated with the TOM complex in mitochondria of human cells. Mol Biol Cell. 2021 [cited 2024 Jan 11];32. Available from: https://pubmed.ncbi.nlm.nih.gov/34347503/.
47. Schmidt O, Harbauer AB, Rao S, Eyrich B, Zahedi RP, Stojanovski D, et al. Regulation of mitochondrial protein import by cytosolic kinases. Cell. 2011 [cited 2024 Jan 11];144:227–39. Available from: https://pubmed.ncbi.nlm.nih.gov/21215441/.
48. Arguello T, Peralta S, Antonicka H, Gaidosh G, Diaz F, Tu YT, et al. ATAD3A has a scaffolding role regulating mitochondria inner membrane structure and protein assembly. Cell Rep. 2021;37: 110139.
49. Chivukula RR, Montoro DT, Leung HM, Yang J, Shamseldin HE, Taylor MS, Dougherty GW, Zariwala MA, Carson J, Daniels MLA, Sears PR, Black KE, Hariri LP, Almogarri I, Frenkel EM, Vinarsky V, Omran H, Knowles MR, Tearney GJ, Alkuraya FS, Sabatini DM. A human ciliopathy reveals essential functions for NEK10 in airway mucociliary clearance. Nat Med. 2020;26(2):244–51. https://doi.org/10.1038/s41591-019-0730-x.
50. Cloonan SM, Choi AMK. Mitochondria in lung disease. J Clin Invest. 2016 [cited 2024 Jan 11];126:809. Available from: https://www.pmc/articles/PMC4767339/.

Publisher's Note